Supporting Information

Ristroph et al. 10.1073/pnas.1000615107

SI Text

Supplementary Movie.

Methods. ***Animal preparation and protocol.*** Animal preparation and protocol: During each day of experiments, about 40 common fruit flies (*D. melanogaster*) from out-bred laboratory strains are first selected for strong flight capability. Each fly is then chilled for 1 to 2 min, and a 1.5 mm cutting of 0.006 inch diameter carbon steel wire (Gordon Brush Co.) is carefully glued to the dorsal surface of the insect's thorax. The adhesive (Norland Optical) is cured for 20 s under ultraviolet light. See Fig. S1 for a photograph of a pinned fly. The insects are then deprived of food and water for approximately 2 h before being inserted into the flight chamber. Filming is then conducted for up to 6 h.

Automated high-speed, three-dimensional videography. See ref. 1 and Fig. S2 for descriptions of the filming apparatus. Three synchronized, orthogonal high-speed cameras (Phantom v7.1, Vision Research, Inc.) record at 8,000 frames per second when triggered by an optical detection system. This frame rate captures about 35 images during each wingstroke, and the magnification is such that the insect body is typically about 80 pixels long. The experimental setup described in ref. 1 is modified by changing the backlighting and introducing the magnetic field system. Specifically, in place of slide projectors, we use bright red light-emitting diodes (LEDs, Diamond Dragon, OSRAM Opto Semiconductor) to backlight each camera. The backlighting and laser (HeNe, Thorlabs) are chosen to be red (wavelength > 600 nm) to minimize the visual stimulus to the insects, which have poor sensitivity to light of long wavelength (2). The magnetic field system includes paired Helmholtz coils placed inside the flight chamber that pass a direct current from a power supply for 5 ms when triggered (Fig. S1). The number of windings in each coil, size and spacing of the coils, and magnitude of the current are chosen to generate a magnetic field strength of about 10^{-2} tesla.

Automated motion tracking. The three-dimensional information contained in the flight videos is analyzed using a recently developed method called hull reconstruction motion tracking (HRMT) (1). HRMT uses the silhouette information captured in the movies to directly reconstruct a representation of the insect's three-dimensional shape. This reconstruction is analyzed to recover the position and orientation of the insect body and wings through time. The difference in the right and left wing angles of attack is used a measure of the wingbeat asymmetry and indicates active torque generation. The angle of attack is defined to be the orientation of the wing measured relative to its velocity. Here, the angle is averaged over each wingstroke and is approximated by the pitch angle η measured relative to the horizontal. Hence, $\Delta\alpha \approx \langle \eta_R - \eta_L \rangle$, where η is the wing pitch angle as measured directly by the HRMT method (1). The approximation is exact in the limit of no stroke plane deviation and is justified by the small deviation for fruit fly wing motions (1, 3).

Control experiments. Movies that capture the flight of insects whose pins had fallen off show no change in behavior upon application of the field, indicating the field alone does not alter flight behavior. Further, experiments conducted with laboratory room lights off show no clear difference from those conducted with lights on. This supports the hypothesis that the mechanosensory halteres, and not the visual system, are responsible for the observed recovery behavior.

Passive Rotational Damping of Symmetrical Flapping Flight. As diagrammed in Fig. 4*A* and *B* of the text, unbalanced drag forces on the flapping wings cause rapid damping of the yaw motion (4–6). Consider an insect of yaw moment of inertia I, average wingbeat angular speed ω, wing area S, and wing span length R. The body itself is rotating with yaw angular velocity $\dot{\psi}$. Because the Reynolds number $\mathrm{Re} = 100$, we use an approximate high-Re fluid force law for the drag force on each wing,

$$D = \frac{1}{2}\rho S u^2 C_D(\alpha), \qquad \textbf{[S1]}$$

where ρ is the density of air, u is the wing speed relative to air, α is the angle of attack of the wing (orientation of wing relative to its velocity), and C_D is the drag coefficient, which depends on α. In a 2D approximation for rotary, flapping wings, we evaluate the drag force at two-thirds span length. Then, the average drag forces on the right and left wings act to give the yaw torque:

$$\frac{1}{2}\rho S C_D(\alpha)\left(\frac{2}{3}R\right)^3[-(\omega+\dot{\psi})^2 + (\omega-\dot{\psi})^2] = -2\left(\frac{2}{3}\right)^3 \rho S C_D(\alpha) R^3 \omega\dot{\psi}. \qquad \textbf{[S2]}$$

Thus, the yaw dynamics are exponentially damped with a damping coefficient β that depends on wing properties:

$$I\ddot{\psi} = -\beta\dot{\psi}, \qquad \beta = 2\left(\frac{2}{3}\right)^3 \rho S C_D(\alpha) R^3 \omega. \qquad \textbf{[S3]}$$

The damping occurs with a characteristic time of about 2 wingbeat periods:

$$\tau = \frac{I}{\beta} \approx 2T. \qquad \textbf{[S4]}$$

In the above calculation, we use approximate morphological and kinematic values obtained from measurements on fruit flies (*D. melanogaster*). For the body: $I = MR_B^2$, with body mass $M = 10^{-6}$ kg and body radius $R_B = 5 \cdot 10^{-4}$ m. For the wings: wing area $S = 2 \cdot 10^{-6}$ m^2 and span length $R = 2 \cdot 10^{-3}$ m. The drag coefficient (7) near $\alpha = 45$ deg is $C_D \approx 2$ and the average flapping angular speed is $\omega = 1100$ s^{-1}. This speed corresponds to a wing flapping with total amplitude sweep of about 140° and with wingbeat period of $T = 4.5$ ms. The fly flaps in air of density $\rho = 1.2$ kg $\cdot$ m^{-3}.

Active Rotational Motion by Rowing Wing Motions. As diagrammed in Fig. 4*C* and *D* of the text, the insect actively turns by inducing differences between the right and left wing angles of attack. The insect initially has equal angles of attack $\alpha_R = \alpha_L = \alpha_0 \approx 45°$. Then, while rowing its wings on the downstroke (Fig. 4*C* and *D*, *Left*), the insect induces differences in the attack angles so that $\alpha_R - \alpha_L = \Delta\alpha$. During the upstroke, the angles then switch to maintain rightward torque (Fig. 4*C* and *D*, *Right*). On average, the drag-based yaw torque sums to give:

$$\frac{1}{2}\rho S\left(\frac{2}{3}R\right)^3[-(\omega+\dot\psi)^2C_D(\alpha_L)+(\omega-\dot\psi)^2C_D(\alpha_R)]$$
$$\approx\frac{1}{2}\rho S\left(\frac{2}{3}R\right)^3[-4\omega\dot\psi C_D(\alpha_0)+\omega^2C'_D(\alpha_0)\cdot\Delta\alpha]$$
$$=-\beta\dot\psi+N_{\mathrm{fly}} \qquad \textbf{[S5]}$$

This calculation approximates the coefficient of drag dependence on angle of attack as $C_D(\alpha)\approx C_D(\alpha_0)+C'_D(\alpha_0)\cdot(\alpha-\alpha_0)$ near $\alpha_0=45°$, which is justified by drag measurements in a dynamically scaled experiment (7). In addition, the terms that are second-order in $\dot\psi$ are negligible because the wing speed is much greater than the body rotational speed: $(\dot\psi/\omega)^2<0.01$, so the neglected terms are $<1\%$ of the retained terms. Thus, the yaw dynamics are again damped with the same damping constant as above and an additional, constant torque is generated by the rowing mechanism:

$$I\ddot\psi=-\beta\dot\psi+N_{\mathrm{fly}}(\Delta\alpha),\qquad \beta=2\left(\frac{2}{3}\right)^3\rho SC_D(\alpha_0)R^3\omega,$$
$$N_{\mathrm{fly}}=\frac{1}{2}\left(\frac{2}{3}\right)^3\rho SC'_D(\alpha_0)R^3\omega^2\cdot\Delta\alpha. \qquad \textbf{[S6]}$$

The torque N_{fly} is thus directly proportional to the angle of attack asymmetry $\Delta\alpha$.

Perfect Correction for Integral Response. The complete yaw dynamics includes inertia, passive rotational damping, active torque generation, and the disturbing torque:

$$I\ddot\psi=-\beta\dot\psi+N_{\mathrm{fly}}(\dot\psi)+N_{\mathrm{ext}}. \qquad \textbf{[S7]}$$

Here, we assume that the insect responds by outputting a torque that depends on its sensory measurement of body angular velocity. If the response is a linear operator on angular velocity, then we can analyze the system using the Laplace transform (8). Taking advantage of the fact that the Laplace transform of the derivative of a function is the frequency times that function, we obtain:

$$Is\dot\psi(s)=-\beta\dot\psi(s)+N_{\mathrm{fly}}(s)\dot\psi(s)+N_{\mathrm{ext}}(s), \qquad \textbf{[S8]}$$

where all functions are now in frequency space and s is the Laplace frequency variable. Assuming a stable system, the Laplace transform of angular velocity is then:

$$\dot\psi(s)=\frac{N_{\mathrm{ext}}(s)}{Is+\beta-N_{\mathrm{fly}}(s)}. \qquad \textbf{[S9]}$$

The requirement for accurate correction is that the total change in yaw angle over all time is zero:

$$\Delta\psi=0=\int_0^\infty\dot\psi dt=\lim_{s\to0}\int_0^\infty e^{-st}\dot\psi dt=\lim_{s\to0}\dot\psi(s). \qquad \textbf{[S10]}$$

Hence, the low-frequency limit of the Laplace transform of angular velocity must be zero. Now, $N_{\mathrm{ext}}(s)$ can be expressed as a series containing terms proportional to s^n with $n\geq0$ for disturbances that last a finite period of time. With regard to recovery, the "worst-case scenario" is that of an impulse: $N_{\mathrm{ext}}(s)$ is a constant ($n=0$). [A disturbance of $N_{\mathrm{ext}}(s)\sim s^n$, for any $n\geq1$, would move the insect and then return it and would thus require no response from the insect.] The simplest controller that guarantees correction after an impulsive disturbance must then have $N_{\mathrm{fly}}(s)\sim1/s$ to satisfy Eqs. **S9** and **S10**. Performing the inverse transform, this operation is the integration over time of the angular velocity (8). Thus, the minimal controller integrates velocity. Note that this argument is unaffected by the presence of delay, which does not alter the long-time (low-frequency) behavior of the system.

1. Ristroph L, Berman GJ, Bergou AJ, Wang ZJ, Cohen I (2009) Automated hull reconstruction motion tracking (HRMT) applied to sideways maneuvers of free-flying insects. *J Exp Biol* 212:1324–1335.
2. Briscoe AD, Chittka L (2001) The evolution of color vision in insects. *Ann Rev Entomol* 46:471–510.
3. Fry SN, Sayaman R, Dickinson MH (2003) The aerodynamics of free-flight maneuvers in *Drosophila*. *Science* 300:495–498.
4. Stengel RF (2004) *Flight dynamics* (Princeton Univ. Press, Princeton).
5. Hesselberg T, Lehmann F-O (2007) Turning behavior depends on frictional damping in the fruit fly *Drosophila*. *J Exp Biol* 210:4319–4334.
6. Hedrick TL, Cheng B, Deng X (2009) Wingbeat time and the scaling of passive rotational damping in flapping flight. *Science* 324:252–255.
7. Dickinson MH, Lehmann F-O, Sane S (1999) Wing rotation and the aerodynamic basis of insect flight. *Science* 284:1954–1960.
8. Bechhoefer J (2005) Feedback for physicists: A tutorial essay on control. *Rev Mod Phys* 77:783–836.

Fig. S1. A common fruit fly (*D. melanogaster*) with ferromagnetic pin glued to the dorsal surface of its thorax is suspended by a magnetized sewing needle. The pin is 1.5 mm long. In free flight, the insect is perturbed by application of a magnetic field that induces a torque on the pin.

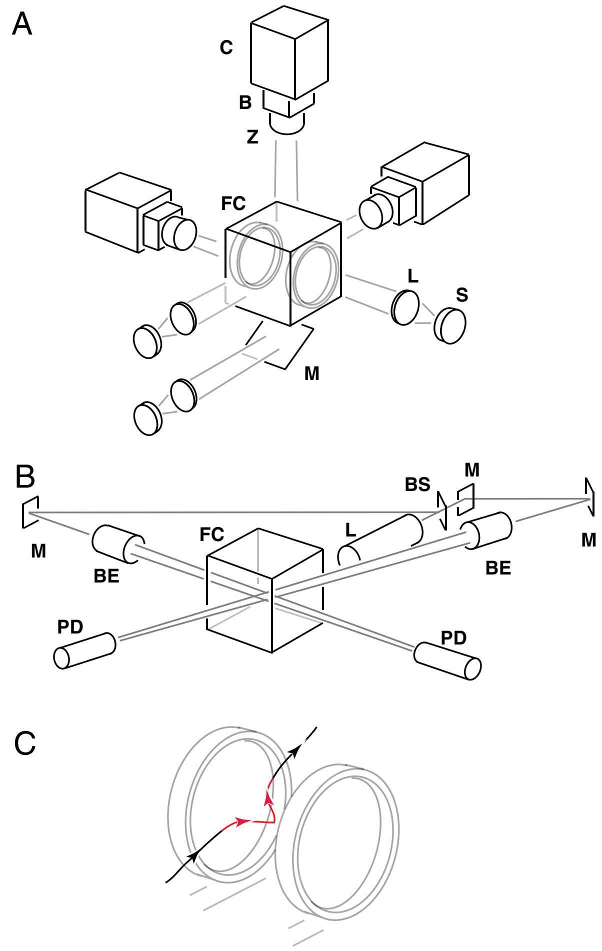

Fig. S2. Schematic of the flight perturbation and videography apparatus. (*A*) Three high-speed cameras (C) focus on a cubic volume (~2 cm side length) in a larger plexiglas flight chamber (FC). The chamber contains a pair of Helmholtz coils that generate a magnetic field. Each camera is fitted with a magnifying bellows (B) and a zoom lens (Z), and each view is backlit by a bright red light-emitting diode source (S) that is focused using a simple convex lens (L). (*B*) An optical triggering system detects the presence of an insect in the filming volume and signals the cameras to record and the magnetic field to turn on. A red laser (L) emits a beam that is divided by a beam splitter (BS), rerouted by mirrors (M), passed through Galilean beam expanders (BE) and the chamber, and focused on photodiodes (PD). When an insect flies through the intersection of the beams, it is detected by the photodiodes, and a triggering circuit (not shown) initiates recording and the application of a magnetic field. (*C*) As an insect flys through the beams, the cameras capture the portion (*Red*) of its trajectory that includes the application of the perturbing field.

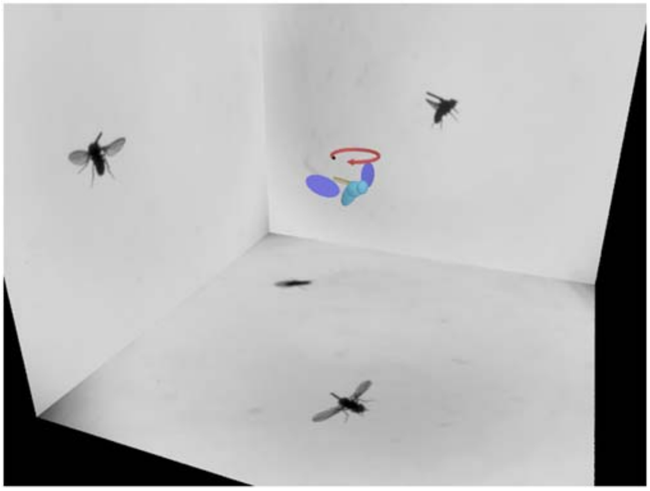

Movie S1.

The flight trajectory of a fruit fly as it recovers from an in-flight perturbation. The side panels display movies captured by three orthogonal high-speed cameras, and the computer-generated insect is reconstructed from these movies. An impulsive magnetic field (*Red Curved Arrow*) torques the ferromagnetic pin (*Bronze Rod*) glued to the insect's thorax and reorients the heading of the fly. The insect responds to this perturbation by making a corrective turn.
Movie S1 (MOV)